Computers and Concrete, *Vol. 26, No. 3 (2020) 275-283*
DOI: https://doi.org/10.12989/cac.2020.26.3.275

Dynamic tensile behavior of SIFRCCs at high strain rates

Seungwon Kim[1a], Cheolwoo Park*[2] and Dong Joo Kim[2b]

[1]*Department of Civil Engineering, Kangwon National University, 346 Jungang-ro, Samcheok 25913, Republic of Korea*
[2]*Department of Civil and Environmental Engineering, Sejong University, 209 Neungdong-ro, Gwangjin-gu, Seoul 05006, Republic of Korea*

(*Received February 24, 2020, Revised August 24, 2020, Accepted August 25, 2020*)

Abstract. Reinforced concrete (RC) does not provide sufficient resistance against impacts and blast loads, and the brittle structure of RC fails to protect against fractures due to the lack of shock absorption. Investigations on improving its resistance against explosion and impact have been actively conducted on high-performance fiber-reinforced cementitious composites (HPFRCCs), such as fiber-reinforced concrete and ultra-high-performance concrete. For these HPFRCCs, however, tensile strength and toughness are still significantly lower compared to compressive strength due to their limited fiber volume fraction. Therefore, in this study, the tensile behavior of slurry-infiltrated fiber-reinforced cementitious composites (SIFRCCs), which can accommodate a large number of steel fibers, was analyzed under static and dynamic loading to improve the shortcomings of RC and to enhance its explosion and impact resistance. The fiber volume fractions of SIFRCCs were set to 4%, 5%, and 6%, and three strain rate levels (maximum strain rate: 250 s^{-1}) were applied. As a result, the tensile strength exceeded 15 MPa under static load, and the dynamic tensile strength reached a maximum of 40 MPa. In addition, tensile characteristics, such as tensile strength, deformation capacity, and energy absorption capacity, were improved as the fiber volume fraction and strain rate increased.

Keywords: slurry-infiltrated fiber-reinforced cementitious composites (SIFRCCs); tensile behavior; dynamic load; explosion and impact resistance; strain rate

1. Introduction

In recent years, damage caused by explosions, collisions, and terrorism has frequently occurred worldwide. With the rapid development of construction technology, structures have become larger and higher, and with the increase of social infrastructures, major national facilities, and business and residential facilities, the occurrence of such unexpected accidents causes massive property loss and human casualties (Kim *et al*. 2017, Kim *et al*. 2018, Kim and Park 2019, Kim *et al*. 2020, Wang *et al*. 2017). The functions of structures have also diversified and become complicated, thereby requiring new measures for protection against explosion and fire (Kim *et al*. 2019, Malvar *et al*. 2007, Wang *et al*. 2017). In particular, understanding the response of structures to extreme loads, such as explosions and shocks is urgently required to enhance the durability of buildings and structures against artificial impacts (Malvar *et al*. 2007, Kim 2017). Moreover, the existing major urban structures are vulnerable to shocks and explosions because they did not consider protection and explosion-proof performance at the time of design and construction (Chan and Chu 2004, Kim 2017, Wang *et al*. 2017). Therefore, it is necessary to evaluate and improve the shock-proof performance of the existing structures, such as important national structures and social infrastructures (Kim, 2017).

Studies on design and safety against explosions and terrorism have been limited to structures and facilities subjected to blast loading, such as the national defense, chemical, and petroleum industries (Banthia and Sappakittipakorn 207, Liu *et al*. 2018, Kim 2017). On the other hand, applying protection and explosion-proof design technologies to high-priority, as well as standard structures, have remained limited (Malvar *et al*. 2007, Kim 2017). For example, in the design of nuclear power plants, which are highly shock-protected structures, a high reinforcement ratio and thick concrete are applied to prevent radiation leakage and the spread of blast due to the loss of coolant accident, but the application of this method to general structures is impracticable in terms of economic efficiency, constructability, and usability (Bindiganavile and Banthia 2005, Choi *et al*. 2018, Kang 2013, Kim 2017). Therefore, it is necessary to develop efficient protection and explosion-proof design and construction technologies that can be widely applied (Kim 2017, Wang *et al*. 2017).

To address these problems, researchers have developed fiber-reinforced composite materials beyond the existing RC structure technology (Poorhosein and Nematzadeh 2018). To improve the fracture of concrete and enhance its explosion and impact resistance, high-performance fiber-reinforced cementitious composites (HPFRCCs), such as fiber-reinforced concrete (FRC) and ultra-high-performance concrete (UHPC) have been studied (Behinaein *et al*. 2018, Lee and Yun 2010, Meraji *et al*. 2019, Nam *et al*. 2016). For

*Corresponding author, Professor
E-mail: tigerpark@kangwon.ac.kr
[a]Assistant Professor
E-mail: seungwon.kim@kangwon.ac.kr
[b]Professor
E-mail: djkim75@sejong.ac.kr

http://www.techno-press.org/?journal=cac&subpage=8 ISSN: 1598-8198 (Print), 1598-818X (Online)

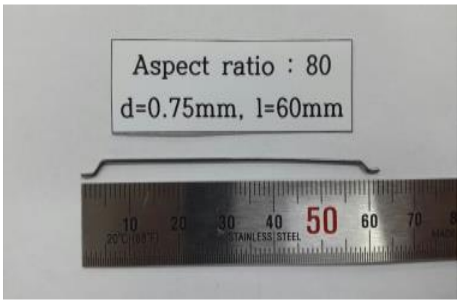

Fig. 1 Steel fiber

these HPFRCCs, however, tensile strength and toughness are still significantly lower compared to their compressive strength, which can reach up to 200 MPa, due to the limited fiber volume fraction (Kim *et al*. 2019, Mosaberpanah and Eren 2017, Poorhosein and Nematzadeh 2018, Park and Lee 2017)

Therefore, in this study, the dynamic tensile behavior of slurry-infiltrated fiber-reinforced cementitious composites (SIFRCCs), which can maximize the fiber volume fraction, was analyzed. The fiber volume fractions of SIFRCCs were set to 4%, 5%, and 6%, and three strain rate levels (maximum strain rate: 250 s^{-1}) were studied. In addition, the static tensile strength was measured for the analysis of behavioral characteristics under dynamic impact loading.

2. SIFRCCs

SIFRCCs used in this study can maximize the fiber volume fraction compared to the existing FRC and HPFRCCs (Kim 2017, Kim *et al*. 2018, Kim *et al*. 2019). Thus, high tensile strength, energy absorption capacity, and deformation capacity can be expected. Unlike conventional FRC and HPFRCCs, SIFRCCs can be prepared by sprinkling steel fibers and then filling with high-performance slurry instead of mixing concrete matrix and steel fibers (Kim 2017, Kim *et al*. 2018, Kim *et al*. 2019). Coarse aggregates are avoided to allow the high-performance slurry to secure sufficient filling performance between the steel fibers (Kim 2017, Kim *et al*. 2018, Kim *et al*. 2019).

3. Experimental procedure

3.1 Materials

In this study, type I ordinary Portland cement and silica fume were used. In addition, fine aggregates with particle diameters of 0.5 mm or less were used to improve the filling performance of the high-performance slurry. It reduces material separation; coarse aggregates were not used to secure the filling performance. A polycarboxylate superplasticizer with high dispersion performance was used to improve the filling performance of the high-performance slurry. The admixtures have high strengths and high fluidity as well as excellent water content reduction and material separation resistance (Kim, 2017; Kim *et al*. 2018; Kim *et al*. 2019).

Hook-ended steel fibers have a 0.75-mm diameter, a 60-mm length, and an 80 aspect ratio, were used. The steel fibers used had a density of 7.8 g/cm^3 and a tensile strength of 1,200 MPa. Fig. 1 shows the steel fiber dimensions of steel fiber.

3.2 Specimen fabrication

For the mixture of SIFRCCs, the water-binder ratio of the high-performance slurry was fixed at 0.35 to fill the

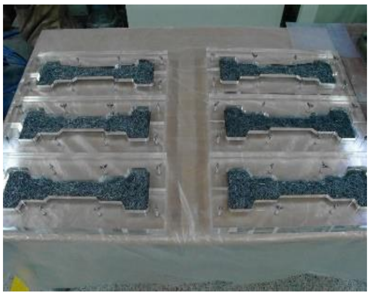

(a) Sprinkling of steel fibers

(b) Slurry filling

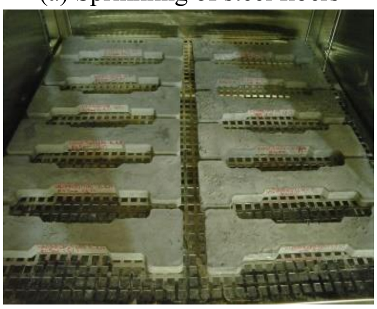

(c) Curing

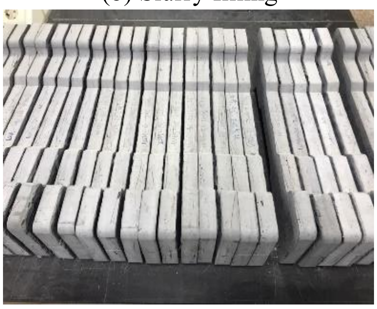

(d) Direct tensile specimens

Fig. 2 Tensile specimen preparation

Table 1 Mixing proportions of SIFRCCs

Variables	Content per unit volume (kg/m^3)						
	W/B (%)	*W*	*C*	Silica fume	Fine aggregate	Superplasticizer	Steel fiber
4%							312
5%	35	407.4	962.8	169.9	566.4	28.3	390
6%							468

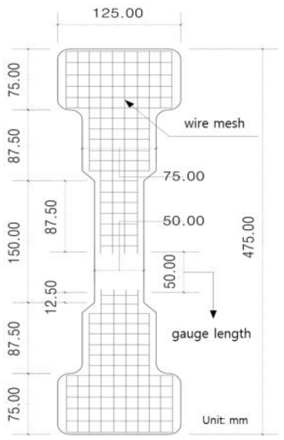

Fig. 3 Specimen drawing

inner space of the steel fibers sprinkled in advance and the content of the superplasticizer was set to 2.5% of the binder weight (Kim 2017, Kim *et al*. 2018, Kim *et al*. 2019). In addition, the content of the fine aggregates was set to 50% of the binder weight and 15% of the cement weight was replaced with silica fume to reduce material separation, and secure required strength (Kim 2017, Kim *et al*. 2018, Kim *et al*. 2019). Table 1 shows the mixing proportions of SIFRCCs used and the fiber volume fraction variables were set to 4%, 5%, and 6%. 40 specimens were prepared for each fiber volume fraction. In addition, 10 test specimens were used for static tensile test, and 30 specimens were used for dynamic tensile test.

Tensile specimens were prepared according to the mixing proportions in Table 1 to analyze the tensile behavior of SIFRCCs with 4%, 5%, and 6% fiber volume fractions. First, the molds were filled with steel fiber with respect to volume fraction. Randomly sprinkled steel fibers in the mold should not overfill the depth of mold and level up as much as possible (Kim *et al*. 2014). The slurry as prepared after mixing the contents was poured until no more bubbles were seen to ensure infiltration of slurry into the fibers because the void has negative effects on the strength of the SIFRCCs. Fig. 2 shows the specimen preparation process.

3.3 Experimental methods

3.3.1 Static tensile strength

The tensile behaviors of SIFRCCs with 4%, 5%, and 6% fiber volume fractions were analyzed. The direct tensile test was conducted by controlling the displacement at a rate of 1 mm/min. Direct tensile specimens in a dog-bone shape suitable for a dedicated tensile equipment were fabricated, as shown in Fig. 3, and their tensile behavior was analyzed

Fig. 4 Scene of the experiment

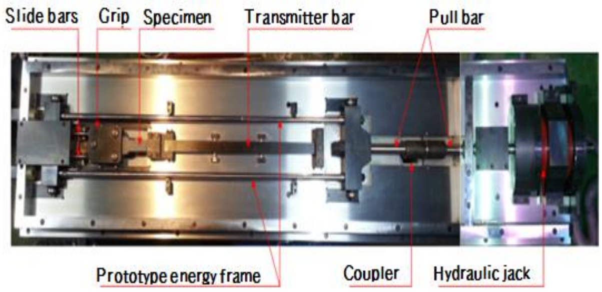

Fig. 5 Improved strain energy frame impact machine (I-SEFIM, Park *et al*. 2017)

using a 300-ton universal testing machine, shown in Fig. 4. The cross-section of a direct tensile specimen with a 50-mm width and a 25-mm height, and the gauge length range to measure tensile performance was set to 50 mm (Kim *et al*. 2019). To induce multiple cracks in SIFRCCs within the gauge length range, wire mesh was installed in all sections expect the gauge length, as shown in Fig. 3. In addition, linear variable differential transformers capable of measuring 25 mm were installed on both sides of the tensile equipment to derive the tensile stress-strain curves of SIFRCCs. The static tensile strength was calculated using Eq. (1).

$$f = \frac{P_{max}}{\text{bh}} \quad (1)$$

where $P_{\max}$ is the maximum load (N), b is the width at the gauge length (mm), and h is the height at the gauge length (mm).

3.3.2 Dynamic tensile strength

The improved strain energy frame impact machine (I-SEFIM) shown in Fig. 5, which was developed by Sejong University, was used to analyze the dynamic tensile behavior of SIFRCCs with respect to fiber volume fraction (Park *et al*. 2017).

To evaluate dynamic tensile behavior under high strain rates, specimens were fabricated by reinforcing wire mesh expect the gap between gauges as shown in Fig. 6(a). Identical gauge lengths were used for the static test. The specimen for dynamic tensile test was prepared by cutting-off one end having reinforced with longer wire mesh as shown in Fig. 6(b).

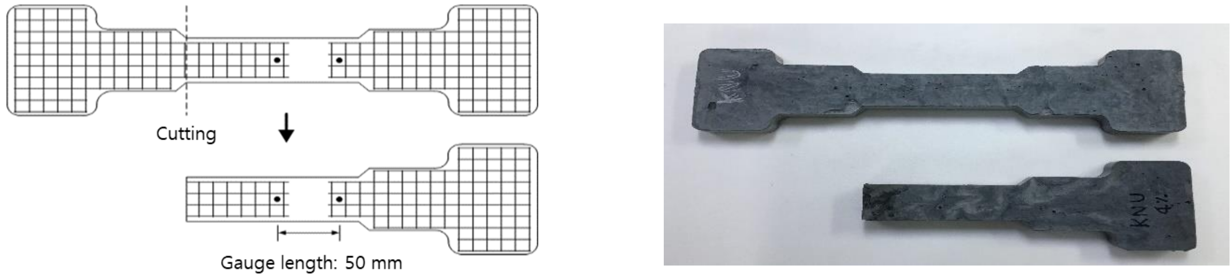

(a) Design of the specimen (b) Preparation of the specimen

Fig. 6 Dynamic tensile specimen reinforced with wire mesh

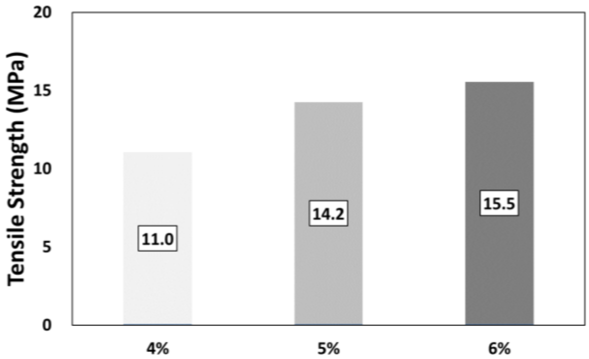

Fig. 7 Tensile strength with fiber volume fraction

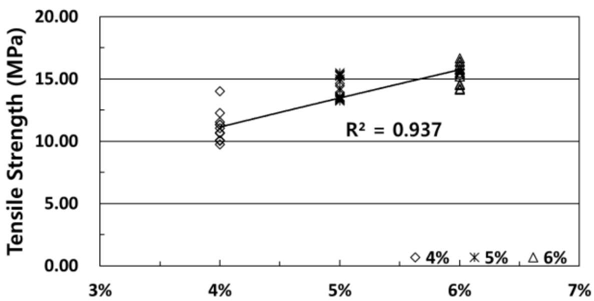

Fig. 8 Change in tensile strength with fiber volume fraction

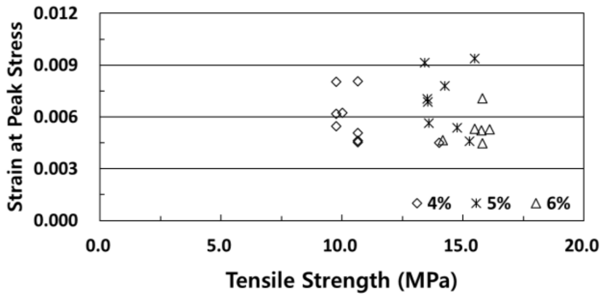

Fig. 9 Deformation capacity at the maximum tensile strength

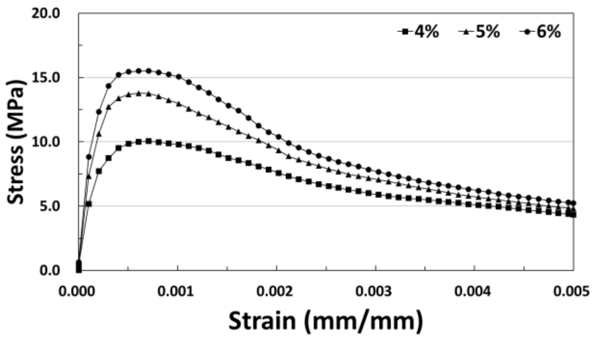

Fig. 10 Tensile stress-strain curve with respect to the fiber volume fraction

In the dynamic tensile test using I-SEFIM, the energy frames store elastic strain energy when the pull bar, which converts the pressure of the energy frames and the hydraulic jack with a maximum capacity of 200 tons into uniaxial tensile force. In addition, as the load applied at the end of pull bar reaches the maximum capacity of the coupler, it is suddenly fractured and the stored elastic strain energy within the energy frame will be rapidly released. The released strain energy produces a high rate stress wave within the frame. The wave propagates through the hinge grip to the specimen and eventually fails the specimen (Park *et al*. 2017, Tran and Kim 2013). The momentary rupture of the coupler converts the stored elastic strain energy into an impact tensile wave. This converted high-speed impact tensile wave is transmitted to the tensile specimen, causing the specimen to rupture. In addition, three strain rate levels - H1 (strain rate below 100 s^{-1}), H2 (strain rate 100-150 s^{-1}), and H3(strain rate above 150 s^{-1}) - were considered.

4. Results and discussion

4.1 Static tensile behavior

4.1.1 Static tensile strength

Figs. 7 and 8 show the tensile strength values of SIFRCCs based on fiber volume fraction. When the fiber volume fraction was 6%, the tensile strength was as high as approximately 15.5 MPa. The tensile strengths were 14.2 and 11.0 MPa when the fiber volume fractions were 5% and 4%, respectively.

The tensile strength test of the SIFRCCs showed that the cracks gradually spread and lead to fracture after the initial cracking due to the reinforcement of steel fibers.

4.1.2 Deformation capacity and tensile stress-strain curve

Fig. 9 shows the deformation capacity experiment results at the maximum tensile strength. The deformation capacity would have also increased as the fiber volume fraction increased because the tensile strength increased; however, the lowest deformation capacity was observed at a

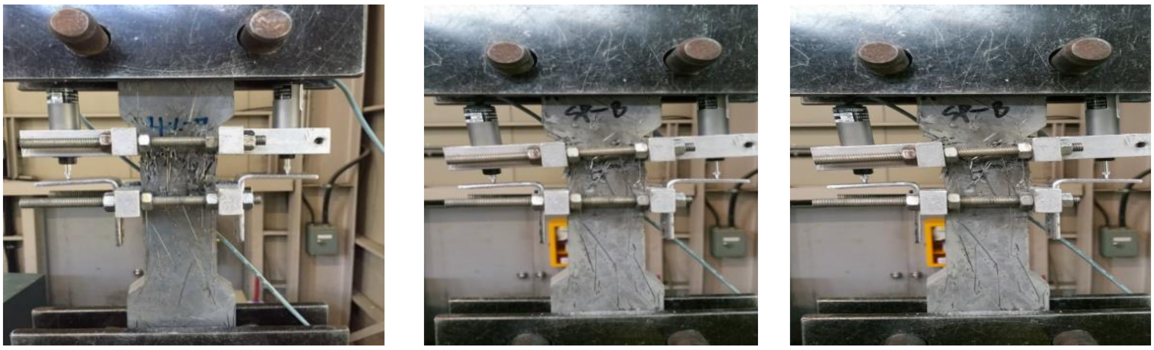

(a) 4% fiber volume fraction (b) 5% fiber volume fraction (c) 6% fiber volume fraction

Fig. 11 Failure of the specimens after static tensile test

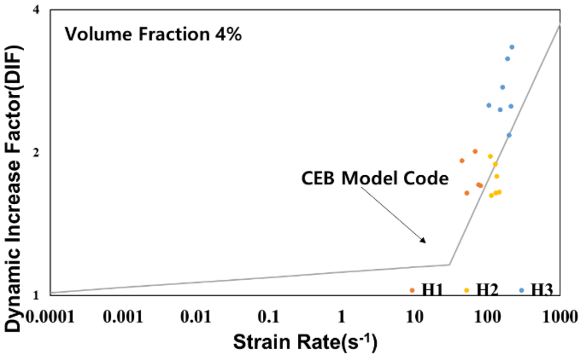

Fig. 12 DIF with respect to the strain rate at 4% fiber volume fraction

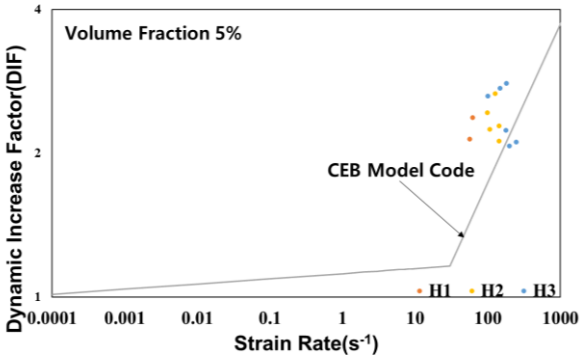

Fig. 13 DIF with respect to the strain rate at 5% fiber volume fraction

6% fiber volume fraction because the degradation of the adhesion between the high-performance slurry and the steel fibers. In addition, considering that the length of the steel fibers used was 60 mm, the deformation capacity appears to have been significantly affected by specimen size because the arrangement of the steel fibers was parallel to the tensile load during the tensile specimen preparation.

Fig. 10 shows the tensile stress-strain curve with respect to the fiber volume fraction of SIFRCCs. When the fiber volume fraction was 6%, the strain was 0.53% (0.0053) and the energy absorption capacity was 62.1 kJ/m^3. When the fiber volume fraction was 5%, the strain was 0.7% (0.0070), exhibiting the highest deformation capacity of all specimens. The energy absorption capacity was also the highest, with an average of 88.1 kJ/m^3. The post-peak behavior characteristic exhibited strain-softening behavior as with the tensile stress-strain test results at 6% fiber volume fraction.

When the fiber volume fraction was 4%, the post-peak behavior characteristic was closest to strain-hardening behavior, unlike the tensile stress-strain test results at 6% and 5% fiber volume fractions. For SIFRCCs with the 4% fiber volume fraction, the energy absorption capacity (approximately 62.3 kJ/m^3) was higher than that with a 6% fiber volume fraction, which showed the highest tensile strength, even though the tensile strength was lower compared to 5% and 6% fiber volume fractions. It appears that different tensile behavior was observed for each specimen because the size of the direct tensile specimens was too small, and the interfacial adhesion between the filling slurry matrix and the steel fibers was not fully developed.

Fig. 11 shows the failure of the test specimens with respect to fiber volume fraction.

4.2 Dynamic tensile behavior

4.2.1 Dynamic tensile strength

Fig. 12 shows the dynamic increase factor (DIF) experimental results with respect to the strain rate at 4% fiber volume fraction. The dynamic tensile strengths at strain rates H1 and H2 were similar. But approximately 10 MPa higher dynamic tensile strength was observed at a higher strain rate of H3. This indicates that the interfacial adhesion between the fibers and high-performance slurry was more developed as the fiber volume fraction decreased and that the dynamic tensile strength increased as the strain rate increased.

Fig. 13 shows the DIF experiment results at 5% fiber volume fraction. The dynamic tensile strength ranged from approximately 32-34 MPa depending on the strain rate.

A small difference was observed for the dependence of dynamic tensile strength on strain rate because the interfacial adhesion strength of each steel fiber decreased as the size of the specimen cross-section was 25×50 mm, and thus the volume of the slurry matrix distributed around the steel fibers was insufficient.

Fig. 14 shows the DIF experimental results at a 6% fiber volume fraction. The average dynamic tensile strength at H3 was found to be approximately 43 MPa, which was 2.76

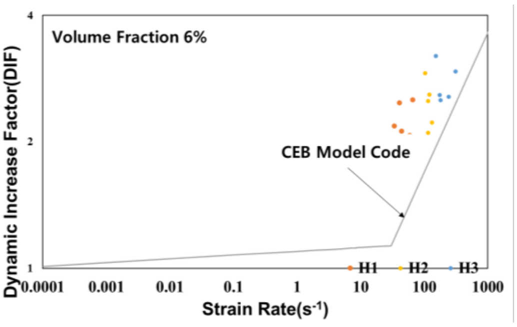

Fig. 14 DIF with respect to the strain rate at 6% fiber volume fraction

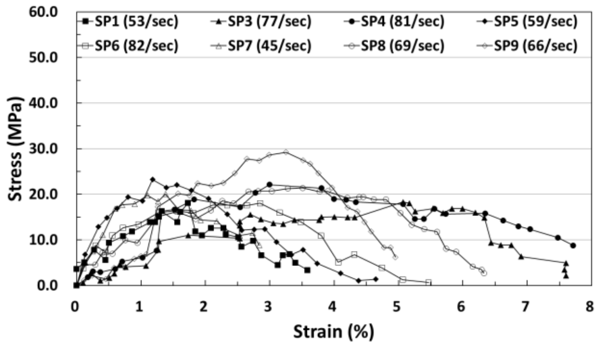

Fig. 16 Stress-strain curve at 4% fiber volume fraction (H1)

(a) 4% fiber volume fraction (b) 5% fiber volume fraction (c) 6% fiber volume fraction

Fig. 15 Failure of the specimens after dynamic tensile test

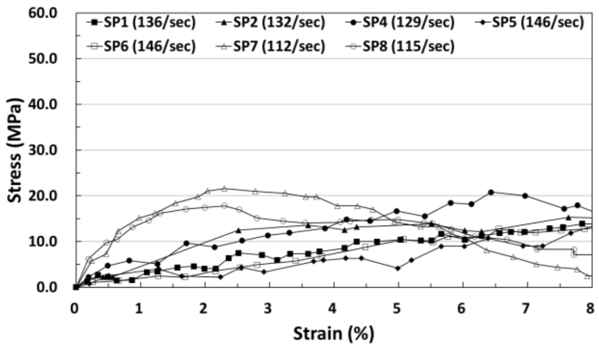

Fig. 17 Stress-strain curve at 4% fiber volume fraction (H2)

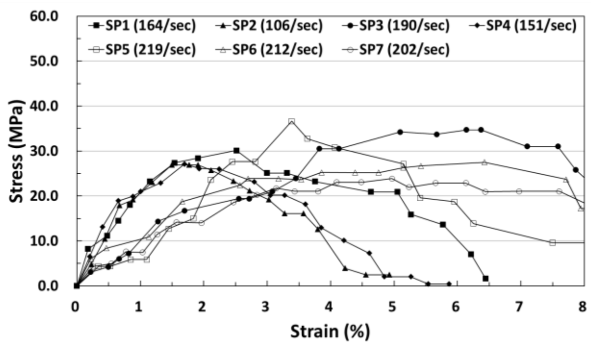

Fig. 18 Stress-strain curve at 4% fiber volume fraction (H3)

times higher than the static tensile strength. The dynamic tensile strengths at H2 and H1 were approximately 38 and 35 MPa. For all variables, DIF was higher than 2.

As the fiber volume fraction in SIFRCCs increased, the dynamic tensile strength tended to increase. The dynamic tensile strength also showed a tendency to increase proportionally as the strain rate increased. In the DIF test results, however, the increase in DIF due to the increase in fiber volume fraction was insignificant. As the fiber volume fraction increased, the increase in dynamic tensile strength with respect to the strain rate was also found to be insignificant. This appears to be because the static tensile strength, which is the basis for deriving DIF, significantly increased as the fiber volume fraction increased. As the strain rate increased, the dynamic tensile strength also increased, but there was no significant change in DIF because the initial appears to have affected the results. The insufficient interfacial adhesion between the steel fibers and the filling slurry matrix due to the insufficient distribution of the matrix around the steel fibers caused by the high fiber volume fraction and the small specimen cross-section primarily determined the results.

Fig. 15 shows the failure of the test specimens with respect to fiber volume fraction.

4.2.2 Deformation capacity and tensile stress-strain curve

When the deformation capacity and energy absorption capacity according to the strain rate were tested at 4% fiber volume fraction, excellent deformation capacity that exceeded 5% was observed at strain rates of H2 and H3. This is nearly nine times higher than the deformation capacity measured during the static tensile test. The energy absorption capacities at H2 and H3 were also found to be 13 times higher than the static tensile test results. It appears that the energy absorption capacity did not increase with strain rate because the specimen was ruptured more easily

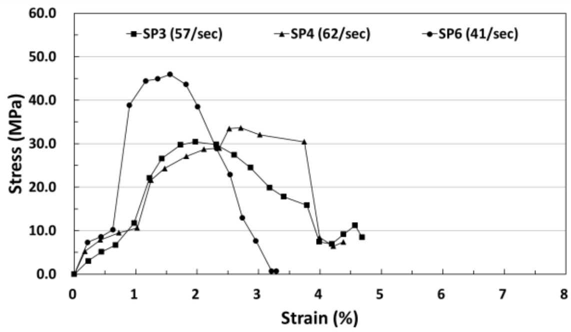

Fig. 19 Stress-strain curve at 5% fiber volume fraction (H1)

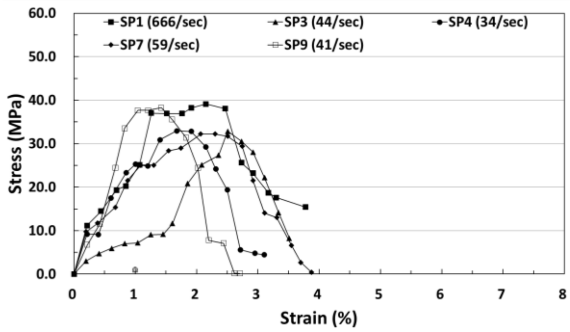

Fig. 22 Stress-strain curve at 6% fiber volume fraction (H1)

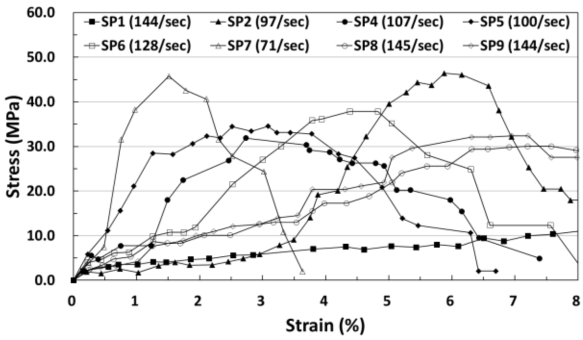

Fig. 20 Stress-strain curve at 5% fiber volume fraction (H2)

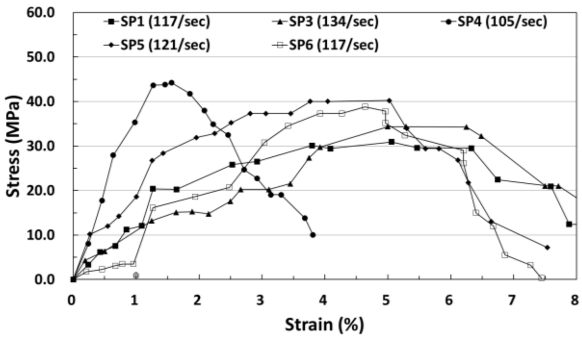

Fig. 23 Stress-strain curve at 6% fiber volume fraction (H2)

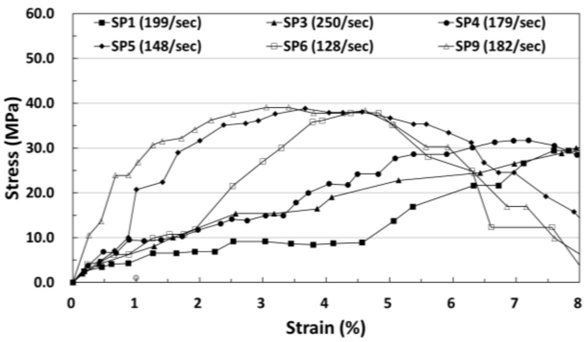

Fig. 21 Stress-strain curve at 5% fiber volume fraction (H3)

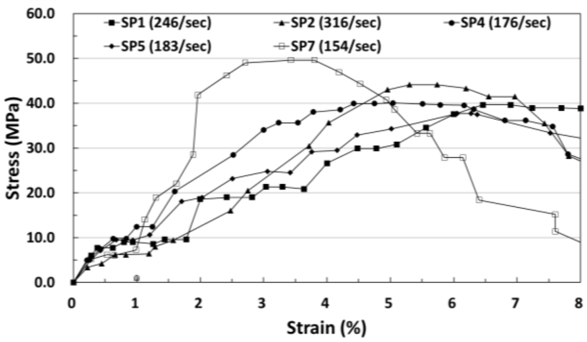

Fig. 24 Stress-strain curve at 6% fiber volume fraction (H3)

under tensile load as the fiber volume fraction decreased. Figs. 16, 17, and 18 show the stress-strain curves at 4% fiber volume fraction.

When the deformation capacity and energy absorption capacity with respect to the strain rate were tested at 5% fiber volume fraction, the tendency of the deformation capacity was similar to that at 6% fiber volume fraction. As the strain rate increased, the deformation capacity increased proportionally. The deformation capacity at 5% fiber volume fraction was found to be similar to that at 6% fiber volume fraction. When the energy absorption capacity was tested at 5% fiber volume fraction, excellent energy absorption capacity, which was approximately 11 times higher than the static energy absorption capacity, was observed at a strain rate of H3. Figs. 19, 20, and 21 show the stress-strain curves at 5% fiber volume fraction.

When the deformation capacity and energy absorption capacity with respect to the strain rate were tested at 6% fiber volume fraction, excellent deformation capacity that exceeded 5% was observed at a strain rate of H3.

When the deformation capacity and energy absorption capacity with respect to the strain rate were tested at 6% fiber volume fraction, excellent deformation capacity that exceeded 5% was observed at a strain rate of H3. In addition, as the strain rate increased, the deformation capacity was improved proportionally. The deformation capacity at H3 was approximately 9 times higher than that measured during the static tensile test. The energy absorption capacity results showed that the energy absorption capacity increased with strain rate as for the deformation capacity test results. In the case of 6% fiber volume fraction, very high energy absorption capacity, 24 times higher than the static energy absorption capacity, was observed due to the integrated behavior of SIFRCCs caused by the input of many steel fibers. Figs. 22, 23, and 24 show the stress-strain curves at 6% fiber volume fraction.

The deformation capacity and energy absorption capacity increased with fiber volume fraction and strain rate, and high deformation capacity exceeding 5% could be observed. It appears that the bridging effect of the steel fibers significantly affected the deformation capacity and energy absorption capacity as the fiber volume fraction increased.

For more accurate analysis of the tensile properties of SIFRCCs with respect to the fiber volume fraction and strain rate, it is deemed necessary to analyze tensile behavior using specimens larger than the ones used in this study so that sufficient interfacial adhesion between the steel fibers and the filling slurry matrix can be obtained.

5. Conclusions

In this study, the tensile behavior of SIFRCCs, which can overcome the shortcomings of HPFRCCs and maximize the fiber volume fraction to respond to shocks (e.g., explosions), was analyzed under static and dynamic loading. The conclusions can be summarized as follows:

- The static tensile behavior of SIFRCCs with high fiber volume fractions was examined. They performed very high maximum tensile strengths, which exceeded 15 MPa. Brittleness, which is a significant shortcoming of conventional concrete, was improved due to the steel fiber reinforcement in large quantities. The initial cracks gradually propagated to reach rupture, and the maximum deformation capacity was approximately 0.7%, indicating excellent energy absorption capacity.
- The bridging effect of the reinforced steel fibers generated strain hardening and multiple cracks, which increased the final crack strength and energy absorption capacity. The deformation capacity was inhibited due to the matrix restraint caused by the increase in adhesion between the matrix and the steel fibers.
- The deformation capacity increased as the fiber volume fraction increased because the tensile strength increased; however, the lowest deformation capacity was observed at a 6% fiber volume fraction because the degradation of the adhesion between the high-performance slurry and the steel fibers.
- When the dynamic tensile behavior of SIFRCCs was analyzed, the energy absorption capacity improved by up to 24 times compared to static loading, and the deformation capacity increased by up to 11 times. In addition, the dynamic tensile strength reached up to 40 MPa, confirming excellent dynamic tensile performance.
- While the dynamic tensile strength increased proportionally as the fiber volume fraction increased, the increase in DIF due to the increasing fiber volume fraction and the increase in dynamic tensile strength due to the increasing strain rate were found to be insignificant because the static tensile strength, which is the basis for deriving DIF, significantly increased as the fiber volume fraction increased. Due to these reasons, it was somewhat challenging to find the tendency of DIF for the dynamic tensile properties of SIFRCCs with respect to the fiber volume fraction. It is necessary to accumulate data and find tendencies through more variable combinations and experiments.
- The evaluation of the dynamic tensile properties of SIFRCCs based on the strain rate is at an early stage. For more accurate property evaluation, it is deemed necessary to identify with more specimens and variables.

Acknowledgments

This research was supported by a grant (20SCIP-B146646-03) from Construction Technology Research Project funded by the Ministry of Land, Infrastructure and Transport of Korea government and by Basic Science Research Program through the National Research Foundation (NRF) of Korea funded by the Ministry of Education (NRF-2019R1I1A1A01062942).

References

Banthia, N. and Sappakittipakorn, M. (2007), “Toughness enhancement in the steel fiber reinforced concrete through fibers hybridization”, *Cement Concrete Res.*, **37**(9), 1366-1372. https://doi.org/10.1016/j.cemconres.2007.05.005.

Behinaein, P., Cotsovos, D.M. and Abbas, A.A. (2018), “Behaviour of steel-fiber-reinforced concrete beams under high-rete loading”, *Comput. Concrete*, **22**(3), 337-353. https://doi.org/10.12989/cac.2018.22.3.337.

Bindiganavile, V. and Banthia, N. (2005), “Generating dynamic crack growth resistance curves for fiber-reinforced concrete”, *Exp. Mech.*, **45**, 112-122. https://doi.org/10.1007/BF02428183.

Chan, Y.W. and Chu, S.H. (2004), “Effect of silica fume on steel fiber bond characteristics in reactive powder concrete”, *Cement Concrete Res.*, **34**(7), 1167-1172. https://doi.org/10.1016/j.cemconres.2003.12.023.

Choi, J.I., Park, S.E., Lee, B.Y. and Kim, Y.Y. (2018), “Tensile properties of polyethylene fiber-reinforced highly ductile composite with compressive strength of 100 MPa class”, *J. Korea Concrete Inst.*, **30**(5), 497-503.

Kang, S.T. (2013), “Bond strength of steel fiber incorporated in ultra high performance fiber-reinforced concrete”, *J. Korea Concrete Inst.*, **25**(5), 547-554. https://doi.org/10.4334/JKCI.2013.25.5.547.

Kim, D.J., Kim, S.W., Yoon, Y.S. and Park, C. (2015), “Impact resistance of strain hardening cementitious composites”, *Mag. Korea Concrete Inst.*, **27**(4), 27-31. https://doi.org/10.22636/MKCI.2015.27.4.27.

Kim, H.S., Kim, G.Y., Lee, S.K., Son, M.J., Choe, G.C. and Nam, J.S. (2019), “Strain rate effects on the compressive and tensile behavior of bundle-type polyamide fiber-reinforced cementitious composites”, *Compos. Part B-Eng.*, **160**, 50-65. https://doi.org/10.1016/j.compositesb.2018.10.008.

Kim, H.S., Kim, G.Y., Lee, S.K., Choe, G.C. and Nam, J.S. (2019), “Direct tensile properties of fiber-reinforced cement based composites according to the length and volume fraction of amorphous metallic fiber”, *J. Korea Inst. Build. Constr.*, **19**(3), 201-207. https://doi.org/10.5345/JKIBC.2019.19.3.201.

Kim, S. (2017), “Strengthening effect on impact resistance of externally reinforced RC member with SIFRCC and FRP”, Ph.D. Dissertation, Kangwon National University, Samcheok.

Kim, S. and Park, C. (2019), “Flexural behavior characteristics of high performance slurry infiltrated fiber reinforced cementitious composite with respect to exposure to high temperature”, *J. Korea Concrete Inst.*, **31**(2), 139-146.

Kim, S., Han, S., Park, C. and Yun, K.K. (2020), “Compressive behavior characteristics of high-performance slurry-infiltrated fiber-reinforced cementitious composites (SIFRCCs) under uniaxial compressive stress”, *Mater.*, **13**(159), 1-13.

https://doi.org/10.3390/ma13010159.
Kim, S., Jung, H., Kim, Y. and Park, C. (2018), "Effect of steel fiber volume fraction and aspect ratio type on the mechanical properties of SIFCON-based HPFRCC", *Struct. Eng. Mech.*, **65**(2), 163-171. https://doi.org/10.12989/sem.2018.65.2.163.
Kim, S., Kim, D.J., Kim, S.-W. and Park, C. (2019), "Tensile behavior characteristics of high-performance slurry-infiltrated fiber-reinforced cementitious composite with respect to fiber bolume fraction", *Mater.*, **12**(3335), 1-11. https://doi.org/10.3390/ma12203335.
Kim, S., Kim, Y., Kim, S.W., Kim, Y.J., and Park, C. (2018), "Strengthening effect of externally reinforced RC structure with SIFRCC on impact load", *Proceeding of ICPS5*, Poznan, August.
Kim, S.W., Park, C.W., Kim, S.W., Cho, H.M., Jeon, S.P. and Ju, M.K. (2014) "Optimum mix proportions of in-fill slurry for high performance steel fiber reinforced cementitious composite", *J. Korean Recy. Constr. Res. Inst.*, **2**(3), 196-201. https://doi.org/10.14190/JRCR.2014.2.3.196.
Lee, Y.O. and Yun, H.D. (2010), "Effects of expansive admixture on the mechanical properties of strain-hardening cement composite (SHCC)", *J. Korea Concrete Inst.*, **22**(5), 617-624. https://doi.org/10.4334/JKCI.2010.22.5.617.
Liu, Q., Zhou, D., Wang, J. and Liu, W. (2018), "Mechanical behavior of FRP confined steel tubular columns under impact", *Steel Compos. Struct.*, **27**(6), 691-702. https://doi.org/10.12989/scs.2018.27.6.691.
Malvar, L.J., Crawford, J.E. and Morrill, K.B. (2007), "Use of composites to resist blast", *J. Compos. Constr.*, **11**, 601-610. https://doi.org/10.1061/(ASCE)1090-0268(2007)11:6(601).
Meraji, L., Afshin, H. and Abedi, K. (2019), "Flexural behavior of RC beams retrofitted by ultra-high performance fiber-reinforced concrete", *Comput. Concrete*, **24**(2), 159-172. https://doi.org/10.12989/cac.2019.24.2.159.
Mosaberpanah, M.A. and Eren, O. (2017), "Statical models for mechanical properties of UHPC using response surface methodology", *Comput. Concrete*, **19**(6), 667-675. https://doi.org/10.12989/cac.2017.19.6.673.
Nam, J.S., Shinohara, Y., Atou, T., Kim, H.S. and Kim, G.Y. (2016), "Comparative assessment of failure characteristics on fiber-reinforced cementitious composite panels under high-velocity impact", *Compos. Part B-Eng.*, **99**, 84-97. https://doi.org/10.1016/j.compositesb.2016.06.008.
Park, J.K., Kim, S.W. and Kim, D.J. (2017), "Matrix-strength-dependent strain-rate sensitivity of strain-hardening fiber-reinforced cementitious composites under tensile impact", *Compos. Struct.*, **162**, 313-324. https://doi.org/10.1016/j.compstruct.2016.12.022.
Park, J.W. and Lee, G.C. (2017), "Effect of compressive strength and curing condition on the direct tensile strength properties of ultra high performance concrete", *J. Korea Inst. Build Constr.*, **17**(2), 175-181. https://doi.org/10.5345/JKIBC.2017.17.2.175.
Park, J.W., Lee, G.C., Koh, K.T. and Ryu, G.S. (2018), "Study on direct tensile properties and reliability review of steel fiber reinforced UHPC", *J. Korea Inst. Build. Constr.*, **18**(2), 125-132. https://doi.org/10.5345/JKIBC.2018.18.2.125.
Poorhosein, R. and Nematzadeh, M. (2018), "Mechanical behavior of hybrid steel-PVA fibers reinforced reactive powder concrete", *Comput. Concrete*, **21**(2), 167-179. https://doi.org/10.12989/cac.2018.21.2.167.
Tran, T.K. and Kim, D.J. (2013), "Investigating direct tensile behavior of high performance fiber reinforced cementitious composites at high strain rates", *Cement Concrete Res.*, **50**, 62-73. https://doi.org/10.1016/j.cemconres.2013.03.018.
Wang, J., Yuan, W., Wu, X. and Wei, K. (2017), "Dynamic performance of girder bridges with explosion-proof and aseismic system", *Struct. Eng. Mech.*, **61**(3), 419-426. https://doi.org/10.12989/sem.2017.61.3.419.

HK